

RESEARCH

Open Access



Autophagy modulation by hADSCs and green light therapy alleviates inflammation and promotes functional recovery after spinal cord injury

Junjie Chen^{1†}, Quanxin He^{1†}, Huan Xie¹, Bin Gu¹, Liyi Zhou¹, Daoyuan Jiang¹, Hongxin Xie², Li Liang², Zhilai Zhou^{1,2*} and Hui Zhang^{1,2*} 

Abstract

Background Spinal cord injury (SCI) results in chronic motor deficits and intractable neuropathic pain, driven by neuroinflammation and impaired tissue repair. Current therapies inadequately address these multifaceted challenges. This study investigated the therapeutic effects of human adipose-derived mesenchymal stem cells (hADSCs) transplantation combined with green light (GL) therapy to modulate inflammation, enhance autophagy, and facilitate functional restoration post-SCI.

Methods In a murine SCI model, hADSCs (1×10^6 cells) were intraspinally delivered with concurrent GL irradiation (100 lux, 8 h/d). Behavioral assessments included footprint analysis, von Frey test, and thermal hyperalgesia testing. Histological analyses included Luxol Fast Blue (LFB), Nissl, Masson, and hematoxylin and eosin (HE) staining for myelin integrity, neuronal survival and glial scar area. Immunofluorescence, ELISA and qPCR were used to assess inflammation, and autophagy-related proteins were analyzed using immunofluorescence and western blotting. The role of microglial autophagy was investigated by inhibiting autophagy using 3-methyladenine (3MA).

Results The combined treatment group (hADSCs + GL) showed significant motor function recovery, pain relief, and histological improvement, outperforming either treatment alone. Histological analyses revealed enhanced myelin preservation, reduced glial scar formation, and increased neuronal survival. Quantitative analysis revealed that TNF- α , IL-1 β , and CD68 expression in the combined treatment group were markedly lower than those in single-treatment cohorts ($P < 0.05$). Furthermore, the combined treatment promoted microglia autophagy, evidenced by increased Beclin1 and LC3B expression and decreased P62 in microglia. Inhibition of autophagy with 3MA reversed the anti-inflammatory benefits of the combined therapy, exacerbating the inflammatory response.

[†]Junjie Chen and Quanxin He have contributed equally to this work.

Co-first authors: Junjie Chen and Quanxin He.

*Correspondence:

Zhilai Zhou
zhouzhilainba@163.com
Hui Zhang
zhanghuixf@163.com

Full list of author information is available at the end of the article



Conclusions The combined treatment of hADSCs transplantation and GL therapy significantly improves functional recovery and reduces inflammation following SCI. The therapeutic effects are mediated in part by the modulation of microglial autophagy.

Keywords Spinal cord injury, Neuropathic pain, Green light, Adipose-derived mesenchymal stem cells, Autophagy

Background

Spinal cord injury (SCI) can cause significant disability, frequently accompanied by neuropathic pain, manifesting as allodynia and hyperalgesia [1–3]. Despite therapeutic advancements, chronic pain remains a significant challenge, profoundly impairing patients' quality of life [4–6]. The complex pathophysiology of SCI, involving neuroinflammation, tissue degeneration, and impaired regeneration, underscores the limitations of current treatments [7, 8]. Pharmacological interventions, such as opioids and anticonvulsants, are often limited by side effects like dependency and tolerance, while non-pharmacological approaches, including physical therapy and neuromodulation, frequently fail to fully restore function or alleviate pain [9, 10]. These limitations highlight the urgent need for innovative therapeutic strategies that address both motor dysfunction and neuropathic pain in SCI.

Human adipose-derived mesenchymal stem cells (hADSCs) emerge as a regenerative therapy for SCI due to their immunomodulatory, tissue-reparative, and anti-inflammatory effects [11–14]. Easily accessible from adipose tissue, hADSCs have demonstrated potential in promoting tissue regeneration and mitigating inflammation in preclinical SCI models [15]. However, the therapeutic efficacy of hADSCs alone is often limited, necessitating the exploration of adjunctive therapies to enhance their potential. Green light (GL) therapy has shown potential for pain management and tissue repair [16–19]. Studies have demonstrated that green light exposure can modulate pain sensitivity pathways and reduce spinal cord inflammation, potentially complementing the effects of hADSCs. For instance, 7-day green light irradiation has been demonstrated to activate glutamatergic and GABAergic neurons in specific brain regions, resulting in analgesic effects in animal models of neuropathic pain [20]. Additionally, preclinical studies report that green light therapy reduces pro-inflammatory cytokines such as TNF- α while enhancing anti-inflammatory mediators like IL10, further supporting its potential in SCI treatment [19].

Within the spinal cord's immune landscape, microglia undergo rapid phenotypic polarization following SCI, transitioning from a homeostatic to a pro-inflammatory state [21–24]. Transcriptomic profiling demonstrates that 78% of microglia in the lesion epicenter adopt an M1-like

phenotype within 24 h post-injury, characterized by upregulated TNF- α /IL-1 β secretion and NLRP3 inflammasome activation [21–24]. Such phenotypic switching directly exacerbates secondary tissue damage and drives chronic neuropathic pain through sustained synaptic sensitization in dorsal horn circuits [25–27]. Autophagy, a cellular process essential for maintaining cellular homeostasis, has recently been implicated in regulating microglial function and neuroinflammation [28, 29]. Enhanced autophagy has been shown to mitigate neuroinflammatory responses and promote neuronal survival, highlighting its promise for therapeutic intervention in SCI [30, 31].

We hypothesize that the combination of hADSCs transplantation and green light therapy may synergistically regulate microglial autophagy, thereby improving motor function and alleviating neuropathic pain in SCI. By targeting both tissue repair and inflammation, this dual approach offers a promising therapeutic strategy to address the complex pathology of SCI.

Materials and methods

The work has been reported in line with the ARRIVE guidelines 2.0.

hADSCs isolation

hADSCs were isolated from excess adipose tissue obtained through liposuction procedures conducted at Guangdong Second Provincial General Hospital. The discarded adipose tissue was collected under ethical approval and patient consent. The tissue was washed extensively with phosphate-buffered saline (PBS) to remove residual blood and debris. The adipose matrix was processed using collagenolytic digestion (type I collagenase, 0.1% w/v, Sigma-Aldrich) under standardized conditions (37 °C, 50 rpm orbital shaking, 60 min). Sequential processing involved initial filtration through a 70 μ m mesh filter (Falcon) to eliminate residual extracellular matrix components, followed by differential centrifugation (1,200 \times g, 10 min, 4 °C) for the stromal vascular fraction isolation. Post-isolation cells were propagated in culture medium (high-glucose DMEM + 10% FBS, Gibco) designed to support stem cell self-renewal. hADSCs were passaged at 80–90% confluence, and their mesenchymal stem cell characteristics were confirmed by flow

cytometry analysis (CD90, CD73, CD105, CD45, CD34, CD14, D19 and HLA-DR).

Identification of hADSCs

Flow cytometry

Flow cytometry was used to detect characteristic surface markers on hADSCs. Passage 3 cells were prepared as single-cell suspensions and subsequently treated using a specialized human mesenchymal stem cell detection kit (TBD-MSFC, Tbdscience). Cellular analysis was conducted on a FACSaria III system (BD Biosciences) in accordance with the manufacturer's guidelines. Approximately 10,000 gated cellular events were recorded and processed through FACSDiva analytical software (BD Biosciences).

Adipogenic differentiation

Adipogenic differentiation was induced using a commercial differentiation medium (PD-006, Pricella). Following a 21-day induction period, intracellular lipid deposition was quantitatively assessed through Oil Red O histochemical analysis. The experimental procedure involved sequential processing steps: cell monolayers were first rinsed with PBS, then chemically fixed using 4% formaldehyde solution for 30 min. Subsequent staining was performed by incubating cells with Oil Red O working solution under ambient laboratory conditions for equivalent duration. To ensure staining specificity, residual dye was thoroughly eliminated through multiple PBS washes. Finally, lipid droplets were microscopically examined using bright field.

Osteogenic differentiation

Osteogenic differentiation was induced using a commercial medium (PD-007, Pricella). Following a 21-day differentiation period, mineralization capacity was determined through Alizarin Red histochemical analysis. The experimental protocol comprised sequential steps: initial PBS rinsing, followed by chemical fixation with 4% paraformaldehyde solution for 30 min. Subsequent staining involved incubation with Alizarin Red working solution equivalent duration. To eliminate nonspecific binding, residual dye was meticulously cleared through three PBS washes. Calcium nodules were visualized under a light microscope.

Chondrogenic differentiation

Chondrogenic differentiation was induced using a commercial chondrogenic differentiation medium (PD-020, Pricella). Following 5-week cultivation, tissues underwent 30-min fixation in 4% neutral buffered formaldehyde.

Specimens were processed through sequential dehydration in graded glucose solutions followed by OCT compound embedding. 5 μ m-thick sections were microtome-generated and adhered to glass substrates. Following triple PBS rinses, tissue sections underwent 30-min incubation with Alcian Blue solution under ambient conditions. Residual dye was eliminated through PBS, washing and the stained cartilage matrix was visualized under a light microscope.

Animals and experimental design

Female C57BL/6 J mice ($n = 245$ total; 6–8 weeks old at study initiation, body weight 18–22 g) were obtained from the SPF-grade Experimental Animal Center of Southern Medical University (Guangzhou, China; Certification SYXK(Yue)2022–0272). Female urinary tract anatomy facilitates catheterization with lower infection risks. Animals were housed in individually ventilated cages (6 mice/cage) under controlled conditions (temperature 22 ± 1 °C, humidity $50 \pm 10\%$) with a 12 h light/dark cycle. Bedding (corn cob) and nesting materials (paper strips) were provided for environmental enrichment. Standard rodent chow and filtered water were available ad libitum. Health status was monitored weekly; no infections or abnormalities were detected pre-experiment. All experimental protocols complied with ethical standards approved by the Animal Ethics Committee of Guangdong Second Provincial General Hospital (Ethics No. 2024-DW-KZ-007–02). The study utilized a two-phase randomized controlled design with individual mice as experimental units. The sample size for each experimental group was determined based on empirical precedents and prior studies in the field [32, 33].

Part 1: therapeutic effects of hADSCs and green light therapy

In this part of the study, the therapeutic effects of hADSCs transplantation combined with GL on SCI were assessed. Animals were assigned to five groups ($n = 37$ /group): SCI (SCI induction without treatment), GL (SCI induction + daily green light therapy, 100 lx, 8 h/day), hADSCs (SCI induction + hADSCs transplantation, 1×10^6 cells in 3 μ L PBS), hADSCs + GL (SCI induction + combined hADSCs transplantation and green light therapy), and Sham (laminectomy without SCI induction). Behavioral assessments, including mechanical hypersensitivity and thermal hyperalgesia, were conducted from SCI induction through the end of the study. Footprint analysis was performed at 35 d.p.i.. Histopathological and molecular assessments were performed at two time points: Day 7 post-injury, when neuroinflammation (TNF- α , IL-1 β , IL-6, IL-18,

IL-10) was quantified via immunofluorescence, qPCR, and ELISA, and autophagy-related markers (P62, Beclin1, LC3B) were assessed by immunofluorescence and Western blot; and Day 35 post-injury, when histopathological repair was evaluated using HE, Nissl, Luxol Fast Blue (LFB) and Masson's trichrome staining, and neuronal survival and axonal regeneration were quantified by NeuN, 5-HT and NF-H immunofluorescence.

Part 2: mechanistic role of microglial autophagy

In the second phase, the functional contribution of microglial autophagy to therapeutic outcomes was examined. Autophagic flux was pharmacologically suppressed through systemic administration of 3-methyladenine (3MA, 15 mg/kg/day i.p.), initiated 24 h post-SCI and maintained for 7 consecutive days. Six groups were included ($n=18$ /group): GL (SCI+green light therapy), GL+3MA (SCI+green light therapy+3MA), hADSCs (SCI+hADSCs transplantation), hADSCs+3MA (SCI+hADSCs transplantation+3MA), hADSCs+GL (SCI+hADSCs transplantation+green light therapy), and hADSCs+GL+3MA (SCI+combined therapy+3MA). On Day 7, autophagy markers (P62, Beclin1, LC3B) were quantified by immunofluorescence, while neuroinflammation was assessed by measuring cytokine levels (IL-10, IL-1 β , TNF- α , IL-18, IL-6) via immunofluorescence, qPCR, and ELISA.

Spinal cord injury modeling

The T10 SCI model was induced as previously described [34, 35]. Anesthesia (isoflurane 2–3%) depth was monitored via pedal reflex suppression. Spinal cord compression was performed bilaterally using 0.1-mm forceps (No. 5 Dumont, Fine Science Tools, USA) for 2 s, ensuring full-width injury without damaging ventral or lateral tissues. Following injury, the muscular and cutaneous layers were surgically closed with interrupted sutures. Postoperative care included thermoregulated recovery (37 °C), ampicillin (30 mg/kg in 100 μ L saline, s.c.), and daily bladder expression until spontaneous urination resumed. At 7- and 35-days post-SCI, isoflurane-anesthetized mice received terminal transcardial perfusion (saline followed by 4% paraformaldehyde) for euthanasia.

hADSCs transplantation

In the experimental cohorts receiving cellular therapy (hADSCs, hADSCs+GL, hADSCs+3MA, hADSCs+GL+3MA), 1×10^6 hADSCs were transplanted in a 3 μ L PBS suspension at the lesion epicenter. The concentration of hADSCs was chosen based on previous studies demonstrating optimal therapeutic outcomes in spinal cord injury models [36, 37]. The procedure utilized

a precision stereotaxic delivery platform (REAWORLD 68528; KD Scientific KDS310Plus) integrated with a 10 μ L microinjection assembly (Hamilton 7653–01 syringe coupled with 33G detachable needle 7803–05). Control groups (SCI, GL, and GL+3MA) received an equivalent volume of PBS following the same procedure.

Green light therapy

The experimental parameters were established based on rodent phototherapy protocols from previous studies [19, 38]. Mice in the green light treatment groups (GL, hADSCs+GL, GL+3MA, and hADSCs+GL+3MA) were housed in custom-designed cages equipped with LED strips (LS-AC50-GR-006, 525 nm wavelength, 8W power output, 120 V input voltage, 120° beam angle) mounted on cage racks. The light intensity was calibrated to 100 lux using a TASI TA8120 lux meter positioned at cage bedding level. During the 8-h daily exposure period (8:00 AM to 4:00 PM), animals were maintained in a light-controlled environment devoid of other illumination sources, with free access to food and water. Mice in other groups were maintained under standard fluorescent lighting in the same room. After behavioral assessments, all mice were returned to their home cages in the animal facility.

Behavioral assessments

Footprint test

Gait recovery and motor coordination were evaluated using the footprint test on day 35 post-SCI. Mice underwent behavioral acclimation in a white paper-lined linear corridor (50 \times 10 cm) prior to testing. Red and blue pigments on mouse forelimbs and hindlimbs, respectively. Footprints were captured using a digital camera and analyzed for overall stepping ability and coordination.

Von frey test

Mechanical nociceptive thresholds were quantified via calibrated von Frey filaments (0.008–2.0 g force range). Mice were acclimated to plexiglass chambers on a mesh floor for 30 min prior to testing. The vonfrey filament vertically stimulated the plantar surface of the hindpaw in ascending order. Each monofilament underwent quintuplicate application, with the nociceptive response threshold operationally defined as the minimum mechanical force inducing $\geq 50\%$ positive paw withdrawal responses across trials.

Hot plate test

Thermal nociception thresholds were assessed using a thermoregulated platform (52.0 °C \pm 0.5 °C), with mice undergoing 5-min habituation to the testing environment

prior to evaluation. Withdrawal latency (time to hind paw lick, flick, or jump) was recorded by blinded observers, with a 30-s cutoff to prevent tissue damage.

Western blotting (WB)

At 7 d.p.i., spinal cord lysates were prepared from three mice per group. 5-mm segments encompassing the lesion were homogenized in RIPA buffer (Beyotime P1050). After centrifugation (15,000×g, 15 min), supernatants were quantified via BCA assay (Beyotime P0010). 50 µg protein/lane was electrophoresed and transferred to PVDF membranes (Millipore ISEQ00010). Membranes were blocked and incubated with: LC3B (1:5000, Abcam ab192890), P62 (1:10,000, Abcam ab109012), Beclin1 (1:5000, Proteintech 66,665-1-Ig), and GAPDH (1:10,000, Cell Signaling Technology 2118). Following secondary antibody incubation, protein bands were visualized through enhanced chemiluminescence (ECL) detection and quantitatively evaluated with ImageJ software.

Quantitative PCR (qPCR)

Spinal cord total RNA was extracted using an RNA extraction kit (M5101, NCM Biotech), followed by RNA quantification. cDNA was synthesized from total RNA using a reverse transcription kit (A232-10, GenStar) and qPCR was performed using a sybr green kit (A301-01, GenStar). Gene expression was normalized to GAPDH and relative expression levels were calculated using the $2^{-\Delta\Delta CT}$ method. Primers used for RT-PCR are listed in Table S1.

ELISA

Pain-related inflammatory factors (IL-10, IL-6, IL-18, IL-1 β , TNF- α) were quantified by ELISA kits (Servicebio GEM0001/02/03/04/10) according to a previous study [39]. Spinal cord homogenates (100 µl) were incubated in antibody-coated plates with detection reagents, followed by TMB substrate reaction. Cytokine levels were determined via 450-nm absorbance measurements (BioTek Synergy H1) and standardized against calibration curves.

Immunofluorescence staining

12 µm-thick longitudinal spinal cord sections underwent sequential immunolabeling pretreatment: initial blocking with 10% donkey serum/0.5% Triton X-100 solution, followed by 16-h incubation at 4 °C with specific immunoglobulin solutions including: NeuN (1:200; Sigma MAB377), NF-H (1:400; Abcam ab8135), 5-HT (1:400; ImmunoStar 20,080), IL-1 β (1:200; Abclonal A22257), TNF- α (1:100; Santa Cruz sc-52746), CD68 (1:200; Bio-Rad MCA1957GA), Iba-1 (1:200/1:500;

Abcam ab283319/Wako 019-19741), P62 (1:400; Abcam ab109012), LC3B (1:200; Abcam ab192890), and Beclin1 (1:400; Proteintech 66,665-1-Ig). Fluorescent secondary antibodies conjugated with Alexa Fluor (1:300, Invitrogen) were incubated for 2 h prior to imaging. Confocal microscopy was conducted using a Leica Stellaris 5 imaging platform for optical section acquisition.

Immunofluorescence quantification

Quantification was performed using Leica X Office software. Fluorescence quantification was systematically performed across three spinal cord regions per specimen (midline and ± 40 µm). The intensity of PKH26, NF-H, 5-HT, TNF- α , IL-1 β , and CD68 was calculated after background signal subtraction. NeuN⁺ cells were manually counted along the rostrocaudal axis (100 µm intervals). Z-stack imaging was employed to assess the colocalization of P62/Beclin1/LC3B with Iba-1⁺ microglia in three fields per section.

Statistical analysis

Data analysis utilized GraphPad Prism 9.0. To minimize observer bias, all behavioral assessments and histopathological evaluations were performed by investigators blinded to group assignments throughout data collection and analysis. Prior to parametric analyses, data normality and variance homogeneity were confirmed. Group differences were assessed via: (1) two-sample t-tests (two groups), or (2) one-/two-way ANOVA with Bonferroni multiple comparisons (≥ 3 groups). The blinding code was only revealed after statistical conclusions were finalized. Values represent mean \pm SD; significance was set at $P < 0.05$.

Results

Isolation, characterization, and transplantation of hADSCs

hADSCs were successfully isolated and cultured in vitro. hADSCs at passage 3 displayed a characteristic spindle-shaped morphology (Fig. 1A). Multilineage differentiation potential was confirmed through Alcian Blue, Oil Red O and Alizarin Red S staining for chondrogenic, adipogenic and osteogenic differentiation, respectively (Fig. 1B–D). Flow cytometry confirmed the mesenchymal stem cell phenotype, with >98% expression of CD90, CD73, and CD105, and <2% expression of CD45, CD34, HLA-DR, CD14 and CD19 (Fig. 1E). To track the transplanted cells, hADSCs were labeled with PKH26 and transplanted into the lesion epicenter. Histological analysis at 35 days post-transplantation showed successful

integration of hADSCs into spinal cord tissue without signs of immune rejection or abnormal proliferation, confirming their survival, distribution, and biological function (Fig. 1F, G).

Combined green light and hADSCs transplantation enhances motor function, alleviates neuropathic pain, and promotes histological repair following SCI

To assess the effects of combined GL and hADSCs transplantation on SCI, we evaluated motor function, neuropathic pain, and histological recovery. Footprint analysis revealed that the SCI group exhibited disorganized footprints, indicative of severe motor dysfunction. In contrast, the combined treatment group demonstrated the most significant recovery, with stable gait and organized stride resembling normal controls (Fig. 2A).

Von Frey test showed that the threshold of foot withdrawal decreased significantly after SCI, and began to rise in each group on the 5 d.p.i. By 7 d.p.i., the combined treatment and hADSCs groups exhibited significantly higher threshold compared to the SCI and GL groups. This trend persisted, with the combined treatment group consistently showing the highest threshold at 14, 21, 28, and 35 d.p.i., indicating superior pain relief (Fig. 2B). Similarly, thermal hyperalgesia testing revealed that the combined treatment group achieved the highest scores at all time points, reflecting the most effective alleviation of pain hypersensitivity (Fig. 2C).

LFB staining demonstrated significant myelin loss in the SCI group and combined treatment group showed the greatest improvement in myelin integrity (Fig. 2D). Nissl staining indicated that neuronal survival in the combined group ($261.1 \pm 23.2/\text{mm}^2$) was closest to sham levels ($363.6 \pm 49.5/\text{mm}^2$), while remaining significantly higher than SCI group levels ($48.4 \pm 11.7/\text{mm}^2$, $p < 0.05$) (Fig. 2D, G). HE staining showed better morphology of the spinal cord in the combined treatment group at 35 days after injury (Fig. 2E). Masson staining revealed that the fibrotic area in the combined treatment group ($0.26 \pm 0.05 \text{ mm}^2$) was significantly reduced compared to the SCI group ($1.85 \pm 0.39 \text{ mm}^2$, $p < 0.05$), with further

statistical superiority over both hADSCs ($0.44 \pm 0.11 \text{ mm}^2$, $p < 0.05$) and GL monotherapy ($0.72 \pm 0.19 \text{ mm}^2$, $p < 0.05$). (Fig. 2F, H). At 35 dpi, the combined group demonstrated superior neuronal distribution and significantly increased NeuN⁺ neuron density compared to the SCI group ($p < 0.05$) (Fig. 3A, D). NF-H⁺ axon density near the lesion core in the combined treatment group ($71.2 \pm 9.5\%$ of sham levels) was significantly increased compared to the SCI group ($24.9 \pm 5.0\%$ of sham; $p < 0.05$), indicating robust axonal regeneration (Fig. 3B, E). Descending 5-hydroxytryptamine (5-HT) axons in combined group recovered to $82.7 \pm 3.4\%$ of sham levels, significantly exceeding hADSCs or GL ($p < 0.05$) (Fig. 3C, F).

Collectively, these findings demonstrate the combined treatment of GL and hADSCs transplantation significantly improves motor function, alleviates neuropathic pain, and enhances histological recovery following SCI, outperforming either treatment alone.

Combined green light and hADSCs treatment reduces inflammation and promotes anti-inflammatory responses

At 7 d.p.i., we evaluated the neuroinflammatory response in spinal cord tissues following various treatments (Fig. 4A–C). Immunofluorescence quantification revealed that TNF- α intensity in the SCI group was reduced by 69% in hADSCs-treated mice ($p < 0.05$ vs. SCI) and 43% in GL-treated mice ($p < 0.05$ vs. SCI). Combined treatment demonstrated the most potent suppression of TNF- α levels, achieving an 78% reduction compared to SCI group ($p < 0.05$). Similar trends were observed for IL-1 β (50% reduction, $p < 0.01$ Combined treatment vs. SCI) (Fig. 4B, E).

Microglial activation (CD68⁺ cells) in the SCI group was attenuated by 74% with combined therapy compared to SCI group ($p < 0.05$). (Fig. 4F). ELISA confirmed elevated anti-inflammatory IL-10 in combined group ($2682.60 \pm 375.05 \text{ pg/mL}$, vs. SCI: $2133.99 \pm 333.43 \text{ pg/mL}$, $p < 0.05$), alongside 72–77% decreases in IL-1 β (77%),

(See figure on next page.)

Fig. 1 Isolation, characterization, and in vivo tracking of hADSCs. **A** Phase-contrast microscopy of P3 hADSCs exhibiting spindle-shaped morphology. **B** Mineralization capacity of hADSCs was evaluated using Alizarin Red S. After 3 weeks of osteoinduction, extracellular calcium deposits (red) were observed in treated cultures. **C** Fat cell formation potential was analyzed via Oil Red O-based lipid quantification assay. Positive staining for neutral lipids (red) was observed in hADSCs cultures subjected to 21 day adipocyte differentiation induction. **D** Chondrogenic differentiation revealed by Alcian Blue staining. Cartilage matrix glycosaminoglycans (blue) were detected in cell aggregates after 5 weeks of induction. **E** Flow cytometry analysis of hADSCs surface markers confirmed a high level of positivity for characteristic mesenchymal markers (CD 105, CD73, CD90 > 98%) and minimal expression of hematopoietic and immune-related markers (CD45, CD34, HLA-DR, CD14 and CD19 < 2%). **F** In vivo distribution of PKH26-labeled hADSCs (red fluorescence) in spinal cord tissue at 35 days post-injury (d.p.i.), demonstrating cellular retention in both hADSCs alone and hADSCs + GL groups. **G** Quantitative analysis of PKH26 fluorescence intensity in the hADSCs and hADSCs + GL groups at 35 days post-transplantation. ($n = 3$, unpaired t-test). ns: no significance

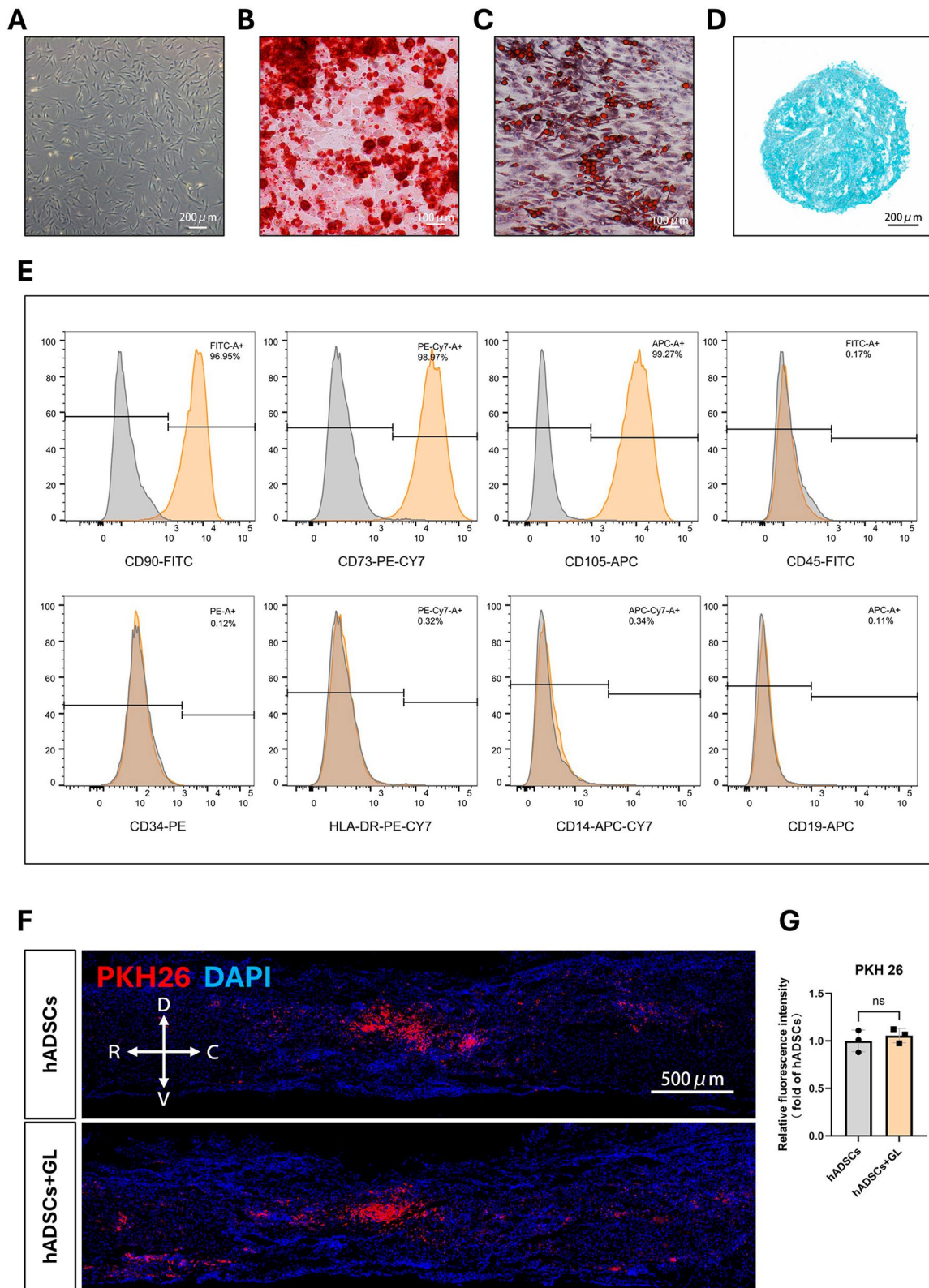


Fig. 1 (See legend on previous page.)

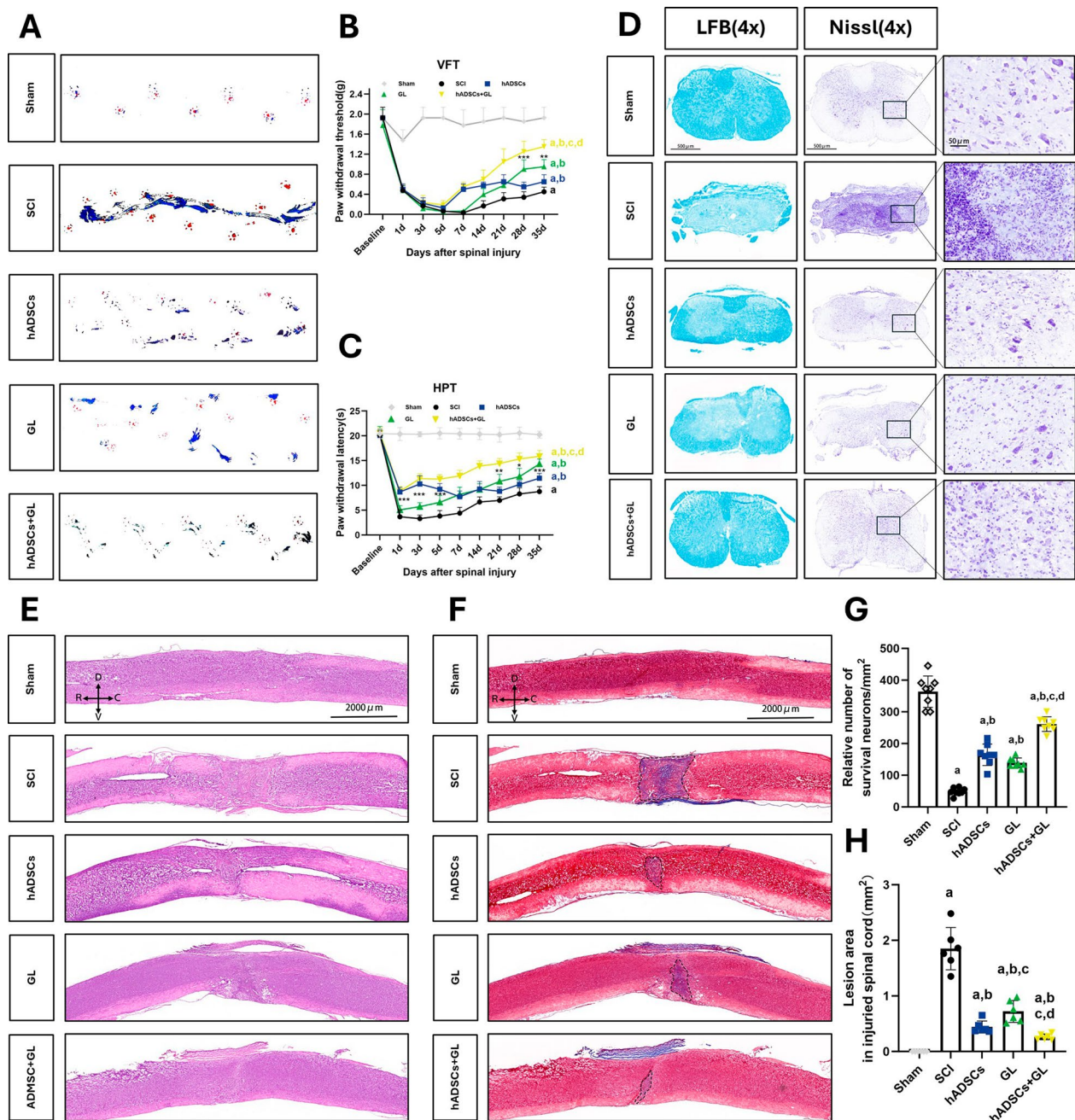


Fig. 2 Combined hADSCs and green light therapy improves functional recovery and histopathological outcomes after SCI. **A** Footprint analysis at 35 d.p.i.. The combined treatment group (hADSCs +GL) exhibited organized strides resembling sham controls. **B** Mechanical allodynia (von Frey test, threshold in g). ($n=8$ mice/group). **C** Thermal hyperalgesia evaluated by hot plate latency (seconds) across the same time points ($n=8$). **D** Spinal cord cross-sections at lesion site (35 dpi). Left: Luxol fast blue (LFB) staining (blue, myelin); Right: Nissl staining (purple, neurons). **E** HE staining of spinal cord longitudinal sections. **F** Masson's trichrome staining. Dashed area: collagen deposition (blue/purple, glial scar). **G** Surviving motor neurons in ventral horn ($n=8$). **H** Fibrotic area quantification ($n=6$). ^a $P < 0.05$ versus Sham, ^b $P < 0.05$ versus SCI, ^c $P < 0.05$ versus hADSCs, ^d $P < 0.05$ versus GL. Bonferroni-adjusted one-way ANOVA

IL-6 (76%), IL-18(72%) and TNF- α (74%) (Fig. 4G). qPCR validated cytokine mRNA reductions (Fig. 4H).

At 35 dpi, combined treatment sustained anti-inflammatory effects, with TNF- α integrated density reduced by 82%, IL-1 β by 70% and CD68 by 84% (Fig. S1).

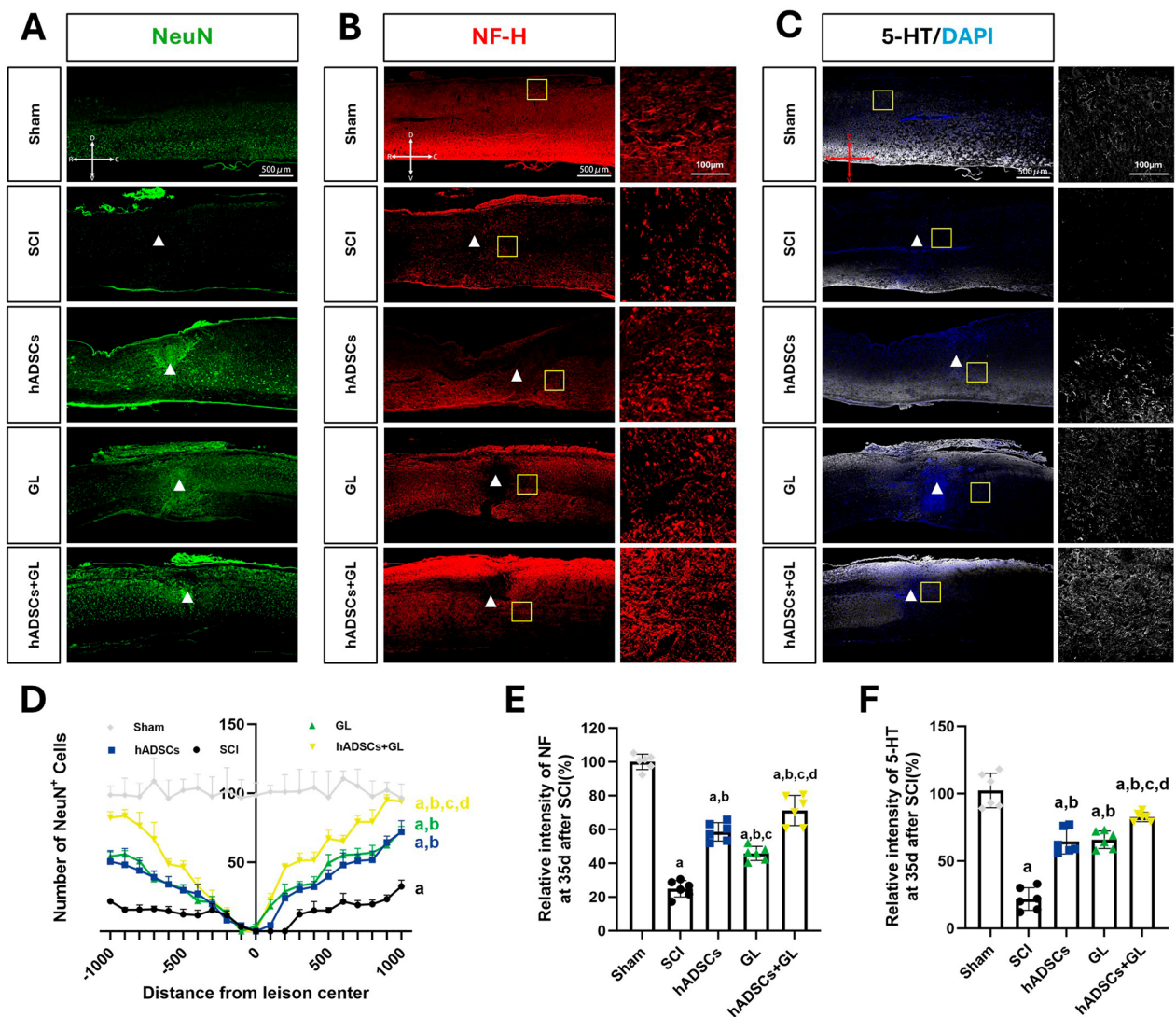


Fig. 3 Combined therapy enhances neuronal survival and axonal regeneration at 35 days post-SCI. **A** Immunofluorescence of NeuN⁺ neurons in longitudinal sections of spinal cords. **B** NF-H⁺ axonal fibers around the lesion epicenter. Boxed region (right) is magnified to highlight fiber density. **C** 5-HT⁺ (serotonergic) axonal fibers in descending tracts. Boxed region (right) is magnified to highlight fiber density. **D** Quantification of NeuN⁺ neurons near the lesion core (n=6). **E** NF-H fluorescence intensity analysis (n=6). **F** 5-HT fluorescence intensity analysis (n=6). ^aP<0.05 versus Sham, ^bP<0.05 versus SCI, ^cP<0.05 versus hADSCs, ^dP<0.05 versus GL. Bonferroni-adjusted one-way ANOVA. White triangle symbols represent the center of spinal cord injury

Synergistic activation of microglial autophagy by combined treatment

At 7 d.p.i., autophagy modulation was assessed by co-staining microglial marker Iba-1 with autophagic markers. Immunofluorescence revealed that SCI increased

p62 accumulation (12.3-fold vs. sham, *p*<0.05), which was reduced by 80% in hADSCs-treated mice (*p*<0.05 vs. SCI) and 63% in GL-treated mice (*p*<0.05). Combined treatment further suppressed p62 (87% reduction, *p*<0.05 vs. SCI). (Fig. 5A, D).

(See figure on next page.)

Fig. 4 Combined therapy synergistically attenuates neuroinflammation at 7 days post-SCI. **A–C** Multiplex immunofluorescence of spinal cord. **A** TNF- α , **B** IL-1 β , **C** CD68⁺ cells. Enlarged views of the area indicated by the dotted box are shown on the right. **D–F** Fluorescence intensity of TNF- α **D**, IL-1 β **E**, and CD68 **F** (n=6) **G** ELISA quantification of cytokines in spinal cord homogenates (pg/mg protein). IL-10: anti-inflammatory; TNF- α /IL-18/IL-6/IL-1 β : pro-inflammatory. **H** RT-qPCR analysis of inflammatory genes normalized to sham. ^aP<0.05 versus Sham, ^bP<0.05 versus SCI, ^cP<0.05 versus hADSCs, ^dP<0.05 versus GL. Bonferroni-adjusted one-way ANOVA

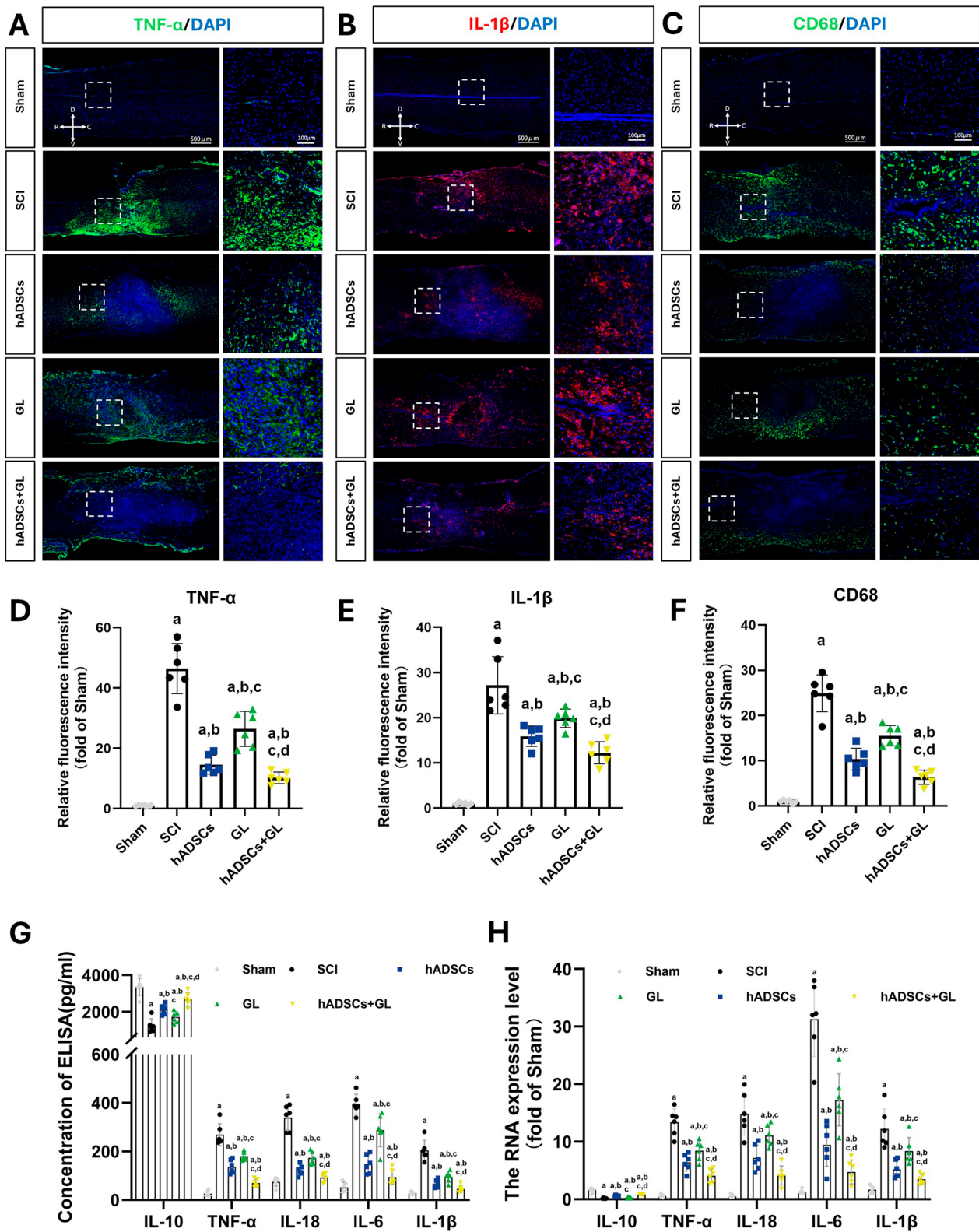


Fig. 4 (See legend on previous page.)

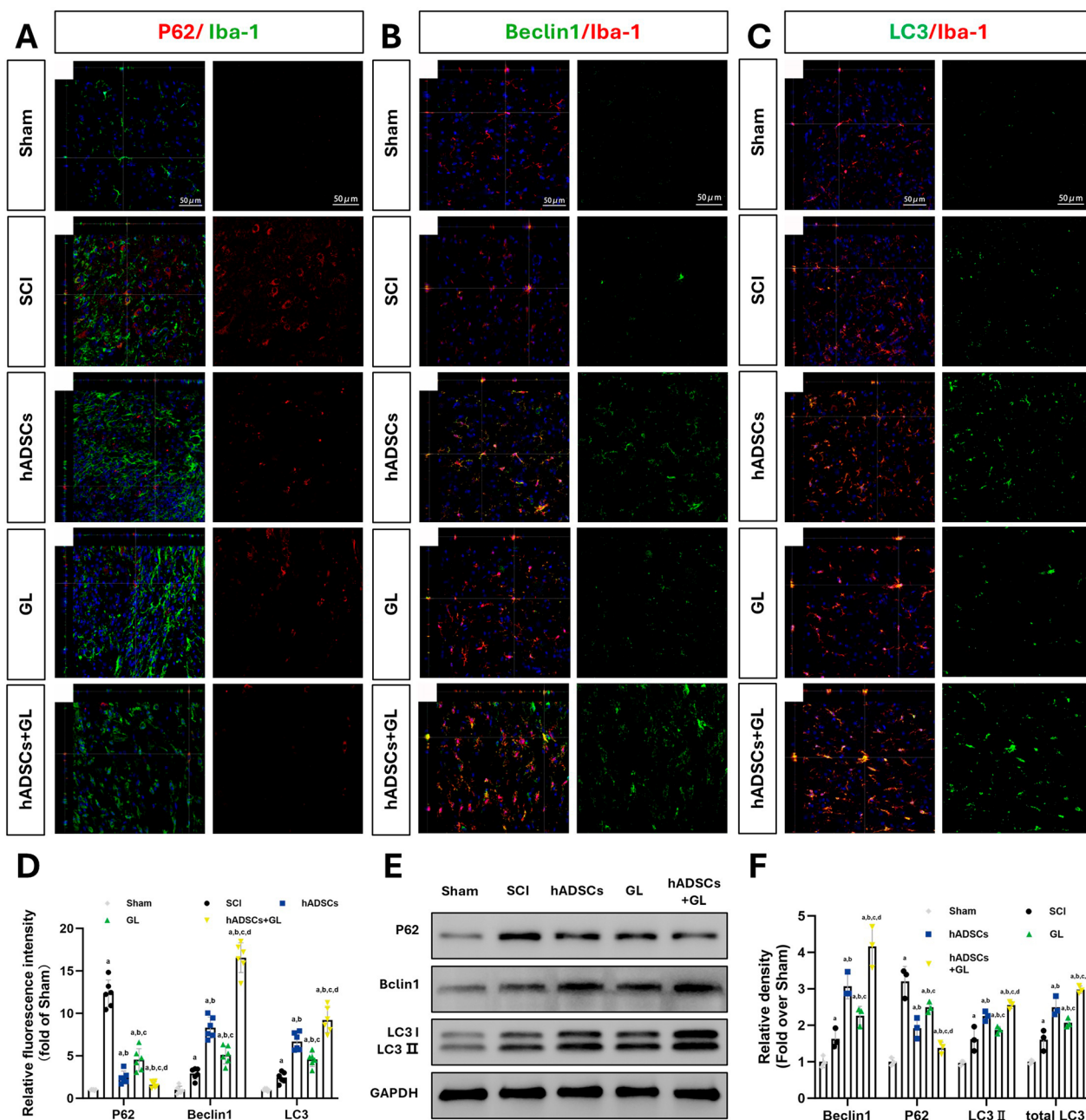


Fig. 5 Combined therapy synergistically activates microglial autophagy at 7 days post-SCI. **(A–C)** Confocal images of spinal cord microglia (Iba-1⁺) co-stained with autophagy markers: **A** p62, **B** Beclin1 and **C** LC3. **D** Quantification of fluorescence intensity in Iba-1⁺ cells (n=6 mice/group). **E** Western blot of LC3, Beclin1, and p62 in spinal cord homogenates. GAPDH served as loading control. Full-length blots are presented in Supplementary Fig. 3. **F** Densitometric analysis of protein levels normalized to GAPDH. ^a*P* < 0.05 versus Sham, ^b*P* < 0.05 versus SCI, ^c*P* < 0.05 vs. hADSCs, ^d*P* < 0.05 vs. GL. Bonferroni-adjusted one-way ANOVA

Conversely, Beclin1 and LC3 levels in SCI group were elevated to 2.9-fold (Beclin1) and 2.7-fold (LC3) by hADSCs, and 1.8-fold (Beclin1) and 1.9-fold (LC3) by GL (*p* < 0.05 vs. SCI). Combined treatment synergistically increased these markers to 5.7-fold (Beclin1) and 3.8-fold (LC3) (*p* < 0.05 vs. SCI) (Fig. 5B–D). Western blot analysis

confirmed these trends: combined therapy reduced p62 to 0.4-fold of SCI levels (*p* < 0.05), increased Beclin1 to 2.5-fold (*p* < 0.05), and elevated LC3B to 1.6-fold (*p* < 0.05) (Fig. 5E, F).

These results indicate that combined therapy synergistically enhances autophagy activation.

Inhibition of autophagy partially reverses the anti-inflammatory benefits of combined hADSCs and green light treatment

To assess whether microglial autophagy mediates the anti-inflammatory effects, we administered 3-methyladenine, a pharmacological inhibitor of autophagosome formation. Immunofluorescence analysis revealed that 3MA treatment significantly increased the fluorescence intensity of P62 while decreasing the fluorescence intensity of Beclin1 and LC3 across all experimental groups (hADSCs+3MA, GL+3MA, and hADSCs+GL+3MA) compared to their respective control (Fig. S2A–D). These findings confirm the effective inhibition of microglial autophagy recovery by 3MA.

This autophagy blockade profoundly exacerbated neuroinflammation. Quantification analysis revealed 2.3–5.2-fold increases in TNF- α , IL-1 β , and CD68 immunoreactivity across 3MA-treated groups relative to vehicle controls (Fig. 6A–F). ELISA quantification demonstrated that 3MA administration abolished IL-10 elevation in hADSCs+GL group (2886.42 ± 626.66 vs. 1932.02 ± 527.53 pg/mg; $P < 0.05$) while amplifying IL-1 β (4.1 \times), IL-6 (3.1 \times), IL-18 (2.5 \times), and TNF- α (2.3 \times) levels (Fig. 6G). Transcriptomic analysis paralleled these findings, showing 7.2–14.6 -fold upregulation of pro-inflammatory cytokine mRNAs and 65.6% suppression of IL-10 expression (Fig. 6H). Collectively, these data establish microglial autophagy as a linchpin mechanism through which combined therapy resolves neuroinflammation post-SCI.

Discussion

Spinal cord injury (SCI) progresses through primary and secondary phases, encompassing acute, subacute, intermediate, and chronic stages [40]. The primary injury involves immediate mechanical disruption of neural and vascular structures, leading to blood–spinal cord barrier compromise and initiating secondary cascades of ischemia, inflammation, and cellular dysfunction [41]. Acute-phase calcium dysregulation and excitotoxicity cause neuronal and glial death, while subacute immune cell infiltration exacerbates tissue damage. In later stages, remyelination, vascular remodeling, and neural reorganization occur [42]. Microglia contribute both to early

debris clearance and to chronic injury via sustained ROS and cytokine release [21].

These pathological changes culminate in chronic paralysis (70% ASIA grade A–C) and disabling neuropathic pain ($VAS \geq 7$), which collectively rank SCI among the most catastrophic neurological disorders in terms of quality-of-life impairment [43, 44]. Despite advancements in therapeutic strategies targeting pain and functional recovery, many patients continue to experience persistent symptoms due to the complex pathophysiology of SCI, which involves neuroinflammation, tissue degeneration, and impaired regeneration [8, 45]. This study investigated the combined therapeutic potential of hADSCs and green light therapy in addressing SCI, focusing on motor function restoration, neuropathic pain reduction, and the modulation of inflammation and autophagy. The results demonstrate that the combined treatment not only enhances functional recovery and alleviates neuropathic pain but also modulates spinal cord inflammation, potentially through the activation of microglial autophagy. These results highlight the promise of combined therapies in addressing both the inflammatory and regenerative aspects of SCI.

Neuroinflammation orchestrates multifaceted pathophysiological cascades post-spinal cord injury, wherein microglia-mediated neural degeneration coincides with maladaptive plasticity underlying chronic nociception [2, 46, 47]. After SCI, the injury site becomes a focal point for inflammation, involving the activation of local microglial cells, the recruitment of immune cells from the periphery, and the secretion of inflammatory mediators [21, 48, 49]. These cytokines exacerbate tissue damage, impede axonal regeneration, and sensitize nociceptors, leading to chronic pain [50, 51]. Our experimental results demonstrated markedly elevated expression levels of pro-inflammatory cytokines within the lesion microenvironment at both 7 days and 35 days post-injury, reflecting the intense inflammatory response post-SCI. The prolonged presence of these cytokines exacerbates tissue destruction and hinders recovery, underscoring the need for therapies that effectively modulate inflammation [52]. Our results show that both hADSCs transplantation and green light therapy individually reduced the expression of pro-inflammatory cytokines, but the combination treatment yielded the most substantial reduction. This

(See figure on next page.)

Fig. 6 Autophagy inhibition by 3MA abolishes the anti-inflammatory effects of combined therapy. **(A–C)** Immunofluorescence of spinal cord longitudinal Sects. (7 d.p.i.) stained for **A** TNF- α , **B** IL-1 β , **C** CD68* cells. **(D–F)** Quantification of fluorescence intensity in lesion center ($n = 6$ mice/group). **G** ELISA of cytokines in spinal cord homogenates (pg/ml). IL-10: anti-inflammatory; others: pro-inflammatory. **H** qPCR analysis of inflammatory genes (*Il-1 β* , *Tnf*, *Il6*) normalized to *Gapdh* (fold-change versus sham; primers in Table S1). * $P < 0.05$, ** $P < 0.01$, *** $P < 0.001$. Bonferroni-adjusted one-way ANOVA

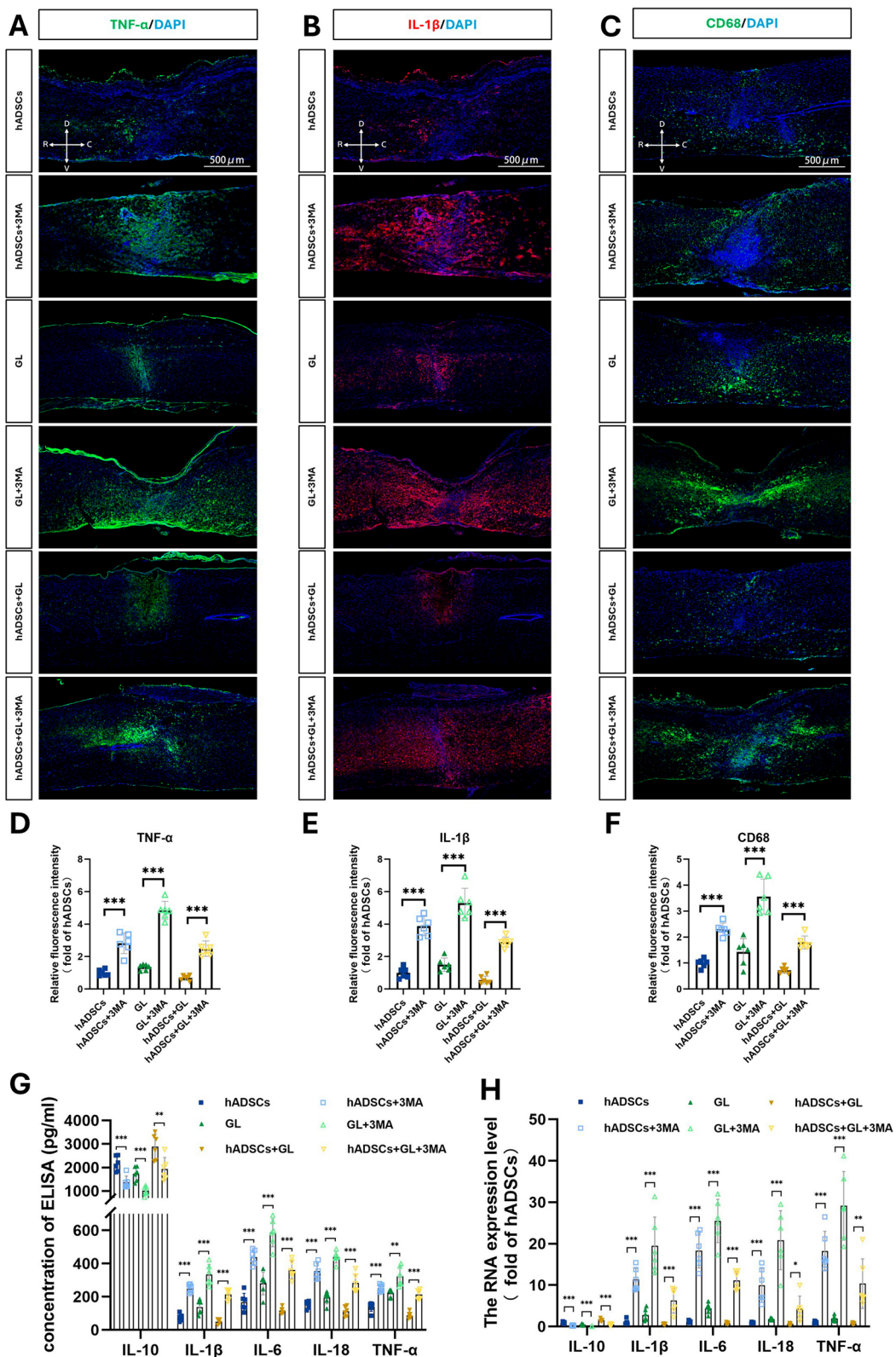


Fig. 6 (See legend on previous page.)

synergistic effect suggests that hADSCs and GL therapy act through complementary mechanisms to mitigate neuroinflammation.

While mesenchymal stem cell (MSC) therapy was traditionally attributed to neural differentiation potential, emerging evidence emphasizes paracrine regulation as the principal mechanism [53]. Our prior findings showing no significant MSC differentiation observed at 28 days post-transplantation in spinal cord injury models corroborate this paradigm shift [36]. Current researches focus on MSC-derived exosomes—nanovesicles transporting proteins, nucleic acids, and lipids—with microRNAs (miRNAs) emerging as critical mediators through multifunctional regulation, including inflammation modulation, dynamic control of microglial/macrophage polarization, enhanced neuronal survival, and facilitation of axonal regeneration [54]. Our other unpublished data further reveal that ADSCs directly secrete specific miRNAs to ameliorate autophagic dysfunction and pyroptosis after spinal cord injury, highlighting their unique mechanism-driven therapeutic advantages.

ADSCs demonstrate translational superiority due to their abundant availability and minimally invasive harvest via lipoaspiration [14]. Clinical trials validate their efficacy: intrathecal administration improved sensory/motor function in 71% (10/14) of SCI patients, with two cases showing restored bowel control, while a recent case study reported a 14-point ASIA score improvement after 10⁸ autologous ADSCs transplantation [55, 56].

Green light (GL) therapy has emerged as a promising noninvasive, cost-effective intervention for chronic pain management. While multiple wavelengths have been explored, green light demonstrates unique therapeutic advantages supported by mechanistic and clinical evidence [18, 19, 38, 57, 58]. GL therapy exerts its anti-inflammatory and analgesic effects through a multimodal mechanism involving both supraspinal and spinal pathways [59]. Clinically, chronic exposure to 100 lux green light (1–2 h/day) has demonstrated efficacy in alleviating diverse chronic pain conditions, including migraine, and fibromyalgia, as evidenced by randomized controlled trials [57, 58, 60]. Experimental evidence identifies visual pathway activation as the primary mediator: (1) Retinal photoreceptor ablation in animal models eliminates GL analgesia, confirming phototransduction necessity; (2) Ocular blockade via opaque lenses abolishes therapeutic effects [16, 18]. These findings establish retinal-to-neural signaling as the fundamental mechanism of GL-mediated pain relief.

At the central nervous system (CNS) level, GL exerts dual effects by enhancing endorphin-mediated nociception suppression while reducing TNF- α and upregulating IL-10 in cerebrospinal fluid. It concurrently

inhibits spinal microglial activation and excitatory neurotransmitter receptor expression, alleviating neuroinflammation and aberrant sensory processing [19]. This neuroimmune-synaptic dual action establishes GL as a novel non-pharmacological therapy for neuropathic pain after SCI. Our data confirm GL's efficacy in attenuating mechanical/thermal hypersensitivity in SCI mice, consistent with reduced spinal inflammation. Although the precise mechanisms through which green light exerts its protective effects are yet to be fully understood, published studies highlight several potential pathways. These include (1) the involvement of the visual system, (2) activation of mu-opioid receptor pathways and descending pain suppression pathways originating from the rostral ventromedial medulla (RVM), (3) an increase in enkephalin expression within the spinal cord, and (4) modifications to the proteomes of both the spinal cord and nociceptors [16].

Notably, our study extends these findings by demonstrating that GL synergizes with hADSCs transplantation to amplify therapeutic outcomes. We propose a bimodal interaction model: (1) GL pretreatment attenuates oxidative stress in the injured spinal cord, creating an immunoregulatory niche characterized by elevated IL-10 and reduced TNF- α , IL-1 β levels; (2) This optimized microenvironment enhances the survival and paracrine activity of transplanted hADSCs. This hypothesis aligns with recent findings that photobiomodulation augments stem cell-derived exosome secretion, warranting further investigation into extracellular vesicle-mediated crosstalk [61, 62].

As specialized immunocompetent cells within the CNS parenchyma, microglia exhibit a context-dependent functional dichotomy during spinal cord injury pathophysiology, simultaneously orchestrating neuroprotective mechanisms and potentiating secondary neurodegeneration [24, 25, 51]. While their activation is initially protective, prolonged activation leads to chronic neuroinflammation, exacerbating neuronal damage and promoting neuropathic pain [23, 63]. Activated microglia release pro-inflammatory cytokines, ROS, and other toxic molecules that hinder tissue repair and axonal regeneration [64]. In our study, the combined treatment significantly reduced CD68 expression, a marker of microglial activation, indicating a reduction in neuroinflammation and its detrimental effects [65]. This reduction likely contributed to the observed improvements in pain relief and functional recovery. Microglial autophagy, a cellular process for degrading and recycling damaged proteins and organelles, has emerged as a critical mechanism in managing neuroinflammation and neuropathic pain following SCI [28, 66, 67]. Restoring microglial autophagy can

alleviate neuroinflammation and promote neuronal survival [67]. Our findings demonstrate that the combined treatment restored microglial autophagy, as evidenced by reduced P62 levels and increased Beclin1 and LC3B expression. This improvement in autophagic activity likely played a role in decreasing inflammatory markers and reducing neuropathic pain [68, 69].

To further elucidate autophagy's role in mediating the therapeutic effects of combined treatment, we employed the autophagy inhibitor 3-methyladenine (3MA) to block microglial autophagy recovery and assess its impact on functional outcomes. 3MA administration significantly increased P62 fluorescence intensity across all experimental groups compared to controls, while markedly reducing Beclin1 and LC3B signals, confirming effective autophagy suppression. Critically, 3MA treatment aggravated neuroinflammation, as evidenced by elevated pro-inflammatory cytokine levels and diminished anti-inflammatory factors, suggesting that autophagy inhibition exacerbates spinal cord inflammation. These findings highlight the essential role of microglial autophagy in mediating the anti-inflammatory actions of combined hADSCs and green light therapy. Although our findings strongly support the contribution of microglial autophagy to the therapeutic benefits of ADSCs combined with green light therapy, additional investigations are required to map the precise autophagic signaling pathways engaged.

Investigating the molecular mechanisms regulating autophagy in microglia will provide valuable insights into optimizing these treatments for clinical applications. Additionally, future studies should explore the downstream effects of autophagy modulation, such as its impact on neuronal survival, axonal regeneration, and functional recovery. The development of targeted therapies that specifically modulate autophagic pathways in microglia could offer a promising strategy for improving SCI outcomes and alleviating chronic neuropathic pain.

In conclusion, microglial autophagy regulation emerges as a novel therapeutic target for SCI. Our findings demonstrate that dual hADSCs and GL therapy enhances microglial autophagy, likely driving the observed attenuation of neuroinflammation and neuropathic pain. Importantly, this autophagic modulation correlates with functional recovery post-SCI. Future investigations delineating the precise molecular mechanisms underlying these effects will be essential to refine targeted interventions and optimize regenerative strategies for SCI rehabilitation.

Conclusion

This research substantiate that recovered autophagic activity in microglia constitutes a pivotal therapeutic strategy, capable of both regulating inflammatory pathways and alleviating neuropathic pain after SCI.

This therapeutic strategy augments autophagic clearance mechanisms, exerting multi-modal neuroprotection through three principal pathways: (1) suppression of neuroinflammatory mediator secretion, (2) mitigate microglial activation, and (3) preservation of spinal cord neuronal integrity. These coordinated cellular responses collectively contribute to the observed alleviation of mechanical allodynia and enhancement of sensorimotor recovery in SCI models.

Abbreviations

SCI	Spinal cord injury
hADSCs	Human adipose-derived mesenchymal stem cells
GL	Green light
LFB	Luxol Fast Blue
HE	Hematoxylin and eosin
3MA	3-Methyladenine
PBS	Phosphate-buffered saline
DMEM	Dulbecco's Modified Eagle Medium
FBS	Fetal bovine serum
FACS	Fluorescence-activated cell sorting
d.p.i.	Days post-injury
cDNA	Complementary DNA
CNS	Central nervous system
MSC	Mesenchymal stem cells

Supplementary Information

The online version contains supplementary material available at <https://doi.org/10.1186/s13287-025-04367-6>.

Supplementary file 1.
Supplementary file 2.
Supplementary file 3.
Supplementary file 4.

Acknowledgements

We are grateful to the Experimental Center of Guangdong Second Provincial General Hospital for providing research facilities and laboratory equipment. We particularly acknowledge Ms. Ling Xiaomei, Ms. Dong Shirui, Ms. Li Jie, and Ms. Zhang Zhen for their expert technical guidance throughout this study. The authors declare that they have not use AI-generated work in this manuscript.

Author contributions

Z.Z and Z.H jointly conceptualized the research framework and established the experimental design. As corresponding authors, both Z.Z and Z.H supervised all aspects of this study, including critical manuscript evaluation and final approval. C.J and H.Q executed in vivo investigations, performed data acquisition and interpretation, as well as participated in manuscript preparation and revision. Technical contributions were provided by X.H, G.B, Z.L, J.D, X.HX and L.L through experimental assistance and methodological consultations. All authors read and approved the final manuscript.

Funding

This research received funding from the Guangzhou Municipal Science and Technology Bureau through two grants: No. 202201010803 (ZLZ) and No. 2024A03J1068 (HZ).

Availability of data and materials

Not Applicable.

Declarations**Ethics approval and consent to participate**

This research does not contain clinical experiments. The procedure for obtaining human cells from hospitals was approved by the ethics committee of The Affiliated Guangdong Second Provincial General Hospital of Jinan University (Approval Number: 2025-KY-KZ-010-02; Title: Green light therapy combined with local injection of mesenchymal stem cells (MSC) in spinal cord improved neuropathic pain in mice after spinal cord injury; Date of approval: 02/08/2025). All the animal experiments are performed at The Affiliated Guangdong Second Provincial General Hospital of Jinan University and approved under the project of "Green light therapy combined with local injection of mesenchymal stem cells (MSC) in spinal cord improved neuropathic pain in mice after spinal cord injury" by the Ethic Committee of The Affiliated Guangdong Second Provincial General Hospital of Jinan University. (Approval Number: 2024-DW-KZ-100-02; Date of approval: 09/26/2024).

Consent for publication

Not Applicable.

Competing interests

The authors declare that they have no competing interests.

Author details

¹The Affiliated Guangdong Second Provincial General Hospital of Jinan University, Guangzhou 510317, Guangdong Province, China. ²The Second School of Clinical Medicine, Southern Medical University, Guangzhou, Guangdong Province, China.

Received: 6 March 2025 Accepted: 24 April 2025

Published online: 22 May 2025

References

- Attal N, Bouhassira D, Baron R. Diagnosis and assessment of neuropathic pain through questionnaires. *Lancet Neurol*. 2018;17(5):456–66.
- Rosner J, de Andrade DC, Davis KD, Gustin SM, Kramer JLK, Seal RP, et al. Central neuropathic pain. *Nat Rev Dis Primer*. 2023;9(1):73.
- Widerström-Noga E. Neuropathic pain and spinal cord injury: management, phenotypes, and biomarkers. *Drugs*. 2023;83(11):1001–25.
- Baastrup C, Finnerup NB. Pharmacological management of neuropathic pain following spinal cord injury. *CNS Drugs*. 2008;22(6):455–75.
- Gurba KN, Chaudhry R, Haroutounian S. Central neuropathic pain syndromes: current and emerging pharmacological strategies. *CNS Drugs*. 2022;36(5):483–516.
- Widerström-Noga E. Neuropathic pain and spinal cord injury: phenotypes and pharmacological management. *Drugs*. 2017;77(9):967–84.
- McDonald JW, Sadowsky C. Spinal-cord injury. *Lancet Lond Engl*. 2002;359(9304):417–25.
- Tian T, Zhang S, Yang M. Recent progress and challenges in the treatment of spinal cord injury. *Protein Cell*. 2023;14(9):635–52.
- Harvey LA. Physiotherapy rehabilitation for people with spinal cord injuries. *J Physiother*. 2016;62(1):4–11.
- Palandi J, Bobinski F, de Oliveira GM, Ilha J. Neuropathic pain after spinal cord injury and physical exercise in animal models: a systematic review and meta-analysis. *Neurosci Biobehav Rev*. 2020;108:781–95.
- Assinck P, Duncan GJ, Hilton BJ, Plemel JR, Tetzlaff W. Cell transplantation therapy for spinal cord injury. *Nat Neurosci*. 2017;20(5):637–47.
- Bydon M, Qu W, Moinuddin FM, Hunt CL, Garlanger KL, Reeves RK, et al. Intrathecal delivery of adipose-derived mesenchymal stem cells in traumatic spinal cord injury: phase I trial. *Nat Commun*. 2024;15(1):2201.
- Andrzejewska A, Dabrowska S, Lukomska B, Janowski M. Mesenchymal stem cells for neurological disorders. *Adv Sci Weinh Baden-Wuert Ger*. 2021;8(7):2002944.
- Liau LL, Looi QH, Chia WC, Subramaniam T, Ng MH, Law JX. Treatment of spinal cord injury with mesenchymal stem cells. *Cell Biosci*. 2020;10:112.
- Chen WC, Liu WF, Bai YY, Zhou YY, Zhang Y, Wang CM, et al. Transplantation of mesenchymal stem cells for spinal cord injury: a systematic review and network meta-analysis. *J Transl Med*. 2021;19(1):178.
- Ibrahim MM, Patwardhan A, Gilbraith KB, Moutal A, Yang X, Chew LA, et al. Long-lasting antinociceptive effects of green light in acute and chronic pain in rats. *Pain*. 2017;158(2):347–60.
- O'Brien MS, Richter E, Woodward T, Bradshaw HB, McDougall JJ. Visual exposure to green light therapy reduces knee joint pain and alters the lipidome in osteoarthritic rats. *Pain*. 2024;166:1274–84.
- Tang YL, Liu AL, Lv SS, Zhou ZR, Cao H, Weng SJ, Zhang YQ. Green light analgesia in mice is mediated by visual activation of enkephalinergic neurons in the ventrolateral geniculate nucleus. *Sci Trans Med*. 2022;14(674):eabq6474. <https://doi.org/10.1126/scitranslmed.abq6474>.
- Martin LF, Cheng K, Washington SM, Denton M, Goel V, Khandekar M, et al. Green light exposure elicits anti-inflammation, endogenous opioid release and dampens synaptic potentiation to relieve post-surgical pain. *J Pain*. 2023;24(3):509–29.
- Wu XQ, Tan B, Du Y, Yang L, Hu TT, Ding YL, et al. Glutamatergic and GABAergic neurons in the vLGN mediate the nociceptive effects of green and red light on neuropathic pain. *Neurobiol Dis*. 2023;183:106164.
- David S, Kroner A. Repertoire of microglial and macrophage responses after spinal cord injury. *Nat Rev Neurosci*. 2011;12(7):388–99.
- Brennan FH, Li Y, Wang C, Ma A, Guo Q, Li Y, et al. Microglia coordinate cellular interactions during spinal cord repair in mice. *Nat Commun*. 2022;13(1):4096.
- Li Y, Ritzel RM, Khan N, Cao T, He J, Lei Z, et al. Delayed microglial depletion after spinal cord injury reduces chronic inflammation and neurodegeneration in the brain and improves neurological recovery in Male mice. *Theranostics*. 2020;10(25):11376–403.
- Jian H, Wu K, Lv Y, Du J, Hou M, Zhang C, et al. A critical role for microglia in regulating metabolic homeostasis and neural repair after spinal cord injury. *Free Radic Biol Med*. 2024;20(225):469–81.
- Sun C, Deng J, Ma Y, Meng F, Cui X, Li M, et al. The dual role of microglia in neuropathic pain after spinal cord injury: detrimental and protective effects. *Exp Neurol*. 2023;370:114570.
- Martini AC, Berta T, Forner S, Chen G, Bento AF, Ji RR, et al. Lipoxin A4 inhibits microglial activation and reduces neuroinflammation and neuropathic pain after spinal cord hemisection. *J Neuroinflammation*. 2016;13(1):75.
- Zhou X, He X, Ren Y. Function of microglia and macrophages in secondary damage after spinal cord injury. *Neural Regen Res*. 2014;9(20):1787–95.
- Li Y, Lei Z, Ritzel RM, He J, Li H, Choi HMC, et al. Impairment of autophagy after spinal cord injury potentiates neuroinflammation and motor function deficit in mice. *Theranostics*. 2022;12(12):5364–88.
- Yang L, Gao X, Tian D, Yang W, Xue S, Cao Z, et al. Resolvin D2 activates anti-inflammatory microglia via restoring autophagy flux and alleviate neuropathic pain following spinal cord injury in rats. *Exp Neurol*. 2023;370:114573.
- Filippone A, Esposito E, Mannino D, Lyssenko N, Praticò D. The contribution of altered neuronal autophagy to neurodegeneration. *Pharmacol Ther*. 2022;238:108178.
- Wu YQ, Xiong J, He ZL, Yuan Y, Wang BN, Xu JY, et al. Metformin promotes microglial cells to facilitate myelin debris clearance and accelerate nerve repairment after spinal cord injury. *Acta Pharmacol Sin*. 2022;43(6):1360–71.
- Xie H, Zhang H, Zhou L, Chen J, Yao S, He Q, et al. Fecal microbiota transplantation promotes functional recovery in mice with spinal cord injury by modulating the spinal cord microenvironment. *J Transl Med*. 2025;23(1):210.
- Fu H, Zhao Y, Hu D, Wang S, Yu T, Zhang L. Depletion of microglia exacerbates injury and impairs function recovery after spinal cord injury in mice. *Cell Death Dis*. 2020;11(7):528.
- Liu K, Lu Y, Lee JK, Samara R, Willenberg R, Sears-Kraxberger I, et al. PTEN deletion enhances the regenerative ability of adult corticospinal neurons. *Nat Neurosci*. 2010;13(9):1075–81.

35. Li Y, He X, Kawaguchi R, Zhang Y, Wang Q, Monavafeshani A, et al. Microglia-organized scar-free spinal cord repair in neonatal mice. *Nature*. 2020;587(7835):613–8.
36. Zhou Z, Tian X, Mo B, Xu H, Zhang L, Huang L, et al. Adipose mesenchymal stem cell transplantation alleviates spinal cord injury-induced neuroinflammation partly by suppressing the Jagged1/Notch pathway. *Stem Cell Res Ther*. 2020;11(1):212.
37. Allahdadi KJ, de Santana TA, Santos GC, Azevedo CM, Mota RA, Nonaka CK, et al. IGF-1 overexpression improves mesenchymal stem cell survival and promotes neurological recovery after spinal cord injury. *Stem Cell Res Ther*. 2019;10(1):146.
38. Martin LF, Moutal A, Cheng K, Washington SM, Calligaro H, Goel V, et al. Green Light Antinociceptive and Reversal of Thermal and Mechanical Hypersensitivity Effects Rely on Endogenous Opioid System Stimulation. *J Pain*. 2021;22(12):1646–56.
39. Zhang Z, Zhu Z, Zuo X, Wang X, Ju C, Liang Z, et al. Photobiomodulation reduces neuropathic pain after spinal cord injury by downregulating CXCL10 expression. *CNS Neurosci Ther*. 2023;29(12):3995–4017.
40. Ahuja CS, Wilson JR, Nori S, Kottler MRN, Druschel C, Curt A, et al. Traumatic spinal cord injury. *Nat Rev Dis Primer*. 2017;27(3):17018.
41. Choo AM, Liu J, Lam CK, Dvorak M, Tetzlaff W, Oxland TR. Contusion, dislocation, and distraction: primary hemorrhage and membrane permeability in distinct mechanisms of spinal cord injury. *J Neurosurg Spine*. 2007;6(3):255–66.
42. Kwon BK, Tetzlaff W, Grauer JN, Beiner J, Vaccaro AR. Pathophysiology and pharmacologic treatment of acute spinal cord injury. *Spine J Off J North Am Spine Soc*. 2004;4(4):451–64.
43. Lu Y, Shang Z, Zhang W, Hu X, Shen R, Zhang K, et al. Global, regional, and national burden of spinal cord injury since 1990 to 2021 and projections for 2050: a systematic analysis for the global burden of disease 2021 study. *Ageing Res Rev*. 2025;103:102598.
44. Lu Y, Shang Z, Zhang W, Pang M, Hu X, Dai Y, et al. Global incidence and characteristics of spinal cord injury since 2000–2021: a systematic review and meta-analysis. *BMC Med*. 2024;22(1):285.
45. Anjum A, Yazid MD, Fauzi Daud M, Idris J, Ng AMH, Selvi Naicker A, et al. Spinal cord injury: pathophysiology, multimolecular interactions, and underlying recovery mechanisms. *Int J Mol Sci*. 2020;21(20):7533.
46. Zrzavy T, Schwaiger C, Wimmer I, Berger T, Bauer J, Butovsky O, et al. Acute and non-resolving inflammation associate with oxidative injury after human spinal cord injury. *Brain J Neurol*. 2021;144(1):144–61.
47. Pfyffer D, Wyss PO, Huber E, Curt A, Henning A, Freund P. Metabolites of neuroinflammation relate to neuropathic pain after spinal cord injury. *Neurology*. 2020;95(7):e805–14.
48. Hanisch UK. Microglia as a source and target of cytokines. *Glia*. 2002;40(2):140–55.
49. Zhang C, Li Y, Yu Y, Li Z, Xu X, Talifu Z, et al. Impact of inflammation and treg cell regulation on neuropathic pain in spinal cord injury: mechanisms and therapeutic prospects. *Front Immunol*. 2024;15:1334828.
50. Hellenbrand DJ, Quinn CM, Piper ZJ, Morehouse CN, Fixel JA, Hanna AS. Inflammation after spinal cord injury: a review of the critical time-line of signaling cues and cellular infiltration. *J Neuroinflammation*. 2021;18(1):284.
51. Chen G, Zhang YQ, Qadri YJ, Serhan CN, Ji RR. Microglia in pain: detrimental and protective roles in pathogenesis and resolution of pain. *Neuron*. 2018;100(6):1292–311.
52. Jin Y, Song Y, Lin J, Liu T, Li G, Lai B, et al. Role of inflammation in neurological damage and regeneration following spinal cord injury and its therapeutic implications. *Burns Trauma*. 2023;11:tkac054.
53. Qi X, Shao M, Peng H, Bi Z, Su Z, Li H. In vitro differentiation of bone marrow stromal cells into neurons and glial cells and differential protein expression in a two-compartment bone marrow stromal cell/neuron co-culture system. *J Clin Neurosci Off J Neurosurg Soc Australas*. 2010;17(7):908–13.
54. Liu WZ, Ma ZJ, Li JR, Kang XW. Mesenchymal stem cell-derived exosomes: therapeutic opportunities and challenges for spinal cord injury. *Stem Cell Res Ther*. 2021;12(1):102.
55. Bydon M, Dietz AB, Goncalves S, Moinuddin FM, Alvi MA, Goyal A, et al. CELLTOP clinical trial: first report from a phase 1 trial of autologous adipose tissue-derived mesenchymal stem cells in the treatment of paralysis due to traumatic spinal cord injury. *Mayo Clin Proc*. 2020;95(2):406–14.
56. Hur JW, Cho TH, Park DH, Lee JB, Park JY, Chung YG. Intrathecal transplantation of autologous adipose-derived mesenchymal stem cells for treating spinal cord injury: a human trial. *J Spinal Cord Med*. 2016;39(6):655–64.
57. Martin L, Porreca F, Mata El, Salloum M, Goel V, Gunnala P, et al. Green light exposure improves pain and quality of life in fibromyalgia patients: a preliminary one-way crossover clinical trial. *Pain Med Malden Mass*. 2021;22(1):118–30.
58. Nelli A, Wright MC, Gulur P. Green light-based analgesia - novel nonpharmacological approach to fibromyalgia pain: a pilot study. *Pain Physician*. 2023;26(4):403–10.
59. Cheng K, Martin LF, Slepian MJ, Patwardhan AM, Ibrahim MM. Mechanisms and pathways of pain photobiomodulation: a narrative review. *J Pain*. 2021;22(7):763–77.
60. Martin LF, Patwardhan AM, Jain SV, Salloum MM, Freeman J, Khanna R, et al. Evaluation of green light exposure on headache frequency and quality of life in migraine patients: a preliminary one-way cross-over clinical trial. *Cephalalgia Int J Headache*. 2021;41(2):135–47.
61. Chang CY, Aviña AE, Chang CJ, Lu LS, Chong YY, Ho TY, et al. Exploring the biphasic dose-response effects of photobiomodulation on the viability, migration, and extracellular vesicle secretion of human adipose mesenchymal stem cells. *J Photochem Photobiol B*. 2024;256:112940.
62. Gholami L, Khorsandi K, Nooshabadi VT, Shahabi S, Jazaeri M, Esfahani H, et al. Effect of photobiomodulation on structure and function of extracellular vesicle secreted from mesenchymal stem cells. *Photochem Photobiol*. 2022;98(6):1447–58.
63. Inoue K, Tsuda M. Microglia in neuropathic pain: cellular and molecular mechanisms and therapeutic potential. *Nat Rev Neurosci*. 2018;19(3):138–52.
64. Kettenmann H, Hanisch UK, Noda M, Verkhratsky A. Physiology of microglia. *Physiol Rev*. 2011;91(2):461–553.
65. Hendrickx DAE, van Eden CG, Schuurman KG, Hamann J, Huitinga I. Staining of HLA-DR, Iba1 and CD68 in human microglia reveals partially overlapping expression depending on cellular morphology and pathology. *J Neuroimmunol*. 2017;15(309):12–22.
66. Liu S, Sarkar C, Dinizo M, Faden AI, Koh EY, Lipinski MM, et al. Disrupted autophagy after spinal cord injury is associated with ER stress and neuronal cell death. *Cell Death Dis*. 2015;6(1):e1582.
67. Liu Y, Chu W, Ma H, Peng W, Li Q, Han L, et al. Fisetin orchestrates neuroinflammation resolution and facilitates spinal cord injury recovery through enhanced autophagy in pro-inflammatory glial cells. *Int Immunopharmacol*. 2024;30(130):111738.
68. Cheng J, Liao Y, Dong Y, Hu H, Yang N, Kong X, et al. Microglial autophagy defect causes parkinson disease-like symptoms by accelerating inflammation activation in mice. *Autophagy*. 2020;16(12):2193–205.
69. Wang ZY, Lin JH, Muharram A, Liu WG. Beclin-1-mediated autophagy protects spinal cord neurons against mechanical injury-induced apoptosis. *Apoptosis Int J Program Cell Death*. 2014;19(6):933–45.

Publisher's Note

Springer Nature remains neutral with regard to jurisdictional claims in published maps and institutional affiliations.